EUROPEAN TRANSACTIONS ON ELECTRICAL POWER
Euro. Trans. Electr. Power 2011; **21**:910–923
Published online 6 September 2010 in Wiley Online Library (wileyonlinelibrary.com). DOI: 10.1002/etep.485

An adaptive neural damping controller for HVDC transmission systems

M. R. Banaei*,† and N. Taheri

Electrical Engineering Department, Faculty of Engineering, Azarbaijan University of Tarbiat Moallem, Tabriz, Iran

SUMMARY

This paper presents a novel linearized model of a power system installed HVAC parallel-connected with a HVDC system based voltage source converter (VSC HVDC) in order to determine the most effective input to apply supplementary controller and design of phase compensator. The power system linearized model cannot be appropriate during the severe disturbances such as three phase faults. In this paper, a nonlinear model of a power system is obtained and in addition, an adaptive neural damping controller based neural identifier is proposed to improve stability and overcome the drawbacks of conventional phase compensator. Simulation results carried out by SIMULINK/MATLAB show the proposed strategy is most effective in comparison with phase compensator. Copyright © 2010 John Wiley & Sons, Ltd.

KEY WORDS: phase compensator; VSC HVDC; neural controller; transient stability

1. INTRODUCTION

HVDC systems interconnect large power systems and offer economic benefits. The usage of these systems includes for example non-synchronous interconnection, control of power flow, and modulation to increase stability limits [1]. The transient stability of the AC systems in a composite AC–DC system can be improved by taking advantage of the fast controllability of HVDC converters [2–4]. Therefore, it is better to construct HVDC links close to HVAC lines.

The VSC HVDC system is the modern HVDC technology. It consists of two VSCs, one of them operates as a rectifier and the other one acts as an inverter. The two converters are connected through a DC line. Its main function is to transmit a constant DC power from the rectifier station to the inverter station, with high controllability [5].

Recently FACTS controllers, such as STATCOM and UPFC, have been used for stability improvement by adding a supplementary signal for main control loops [6,7].

In this paper, a HVAC system in a parallel VSC HVDC system has been modeled as nonlinear state space equations and then these equations have been linearized around operating point in order to analyze the small-signal stability of the system and to design phase compensator. These phase compensator parameters are set for particular operating point, therefore the controller parameters tune cannot guarantee its performance in another operating point. Also, it may not be able to suppress oscillations resulted from severe disturbances, especially those three-phase faults which may occur at the generator terminals. Adaptive neural networks have been successfully applied to the identification and control of nonlinear systems because they have the advantages of high computation speed, generalization, and learning ability. In Reference [8], a neural controller has been used to regulate parameters of a classic PSS and in Reference [9] it has been applied for transient stability enhancement

*Correspondence to: M. R. Banaei, Electrical Engineering Department, Faculty of Engineering, Azarbaijan University of Tarbiat Moallem, Tabriz, Iran.
†E-mail: m.banaei@azaruniv.edu

using UPFC. In Reference [10,11], two neural networks have been used to design a power system stabilizer. One of these neural networks acts as an identifier and the other one acts as a controller. In this paper, a novel nonlinear model is presented for a power system installed with VSC HVDC and then a supplementary neural damping signal is added to rectifier phase angle input, which this input has been selected using singular value decomposition (SVD) method as effectiveness control signal. The online training method is applied to training the controller through neural identifier and then the performance of supplementary neural controller, which can be tuned for overall operating points, is compared with phase compensator.

2. POWER SYSTEM INSTALLED WITH HVDC

Figure 1 shows a single machine infinite bus (SMIB) system equipped with an HVDC. As it can be seen, the infinite bus is supplied by HVAC parallel connected with a HVDC power transmission system. The HVDC consists of two coupling transformer, two three-phase IGBT based voltage source converters (VSCs). Theses two IGBT VSCs are connected by a DC transmission line.

The four input control signals to the HVDC are M_r, $\mathrm{PH_r}$, M_i, $\mathrm{PH_i}$ where M_r, M_i are the amplitude modulation ratio and $\mathrm{PH_r}$, $\mathrm{PH_i}$ are phase angle of the control signals of rectifier and inverter, respectively. The AC side of each converter is connected to the line through a coupling transformer. The first VSC behaves as a rectifier. It regulates the DC link voltage and maintains the magnitude of the voltage at the connected terminal by two input control signals, M_r, $\mathrm{PH_r}$. The second VSC acts as a controlled voltage source, which controls power flow in HVDC feeder by controlling M_i, $\mathrm{PH_i}$.

2.1. Modeling of power system

By applying Park's transformation and neglecting the resistance and transients of the coupling transformers, the HVDC can be modeled as:

$$\begin{bmatrix} V_{\mathrm{ld}} \\ V_{\mathrm{lq}} \end{bmatrix} = \begin{bmatrix} 0 & X_{\mathrm{s}} \\ -X_{\mathrm{s}} & 0 \end{bmatrix} \begin{bmatrix} I_{\mathrm{old}} \\ I_{\mathrm{olq}} \end{bmatrix} + \begin{bmatrix} \frac{M_{\mathrm{r}} V_{\mathrm{dcr}} \cos(\mathrm{PH_r})}{2} \\ \frac{M_{\mathrm{r}} V_{\mathrm{dcr}} \sin(\mathrm{PH_r})}{2} \end{bmatrix} \tag{1}$$

$$\begin{bmatrix} V_{\mathrm{bd}} \\ V_{\mathrm{bq}} \end{bmatrix} = \begin{bmatrix} 0 & X_{\mathrm{sp}} \\ -X_{\mathrm{sp}} & 0 \end{bmatrix} \begin{bmatrix} I_{\mathrm{obd}} \\ I_{\mathrm{obq}} \end{bmatrix} + \begin{bmatrix} \frac{M_{\mathrm{i}} V_{\mathrm{dci}} \cos(\mathrm{PH_i})}{2} \\ \frac{M_{\mathrm{i}} V_{\mathrm{dci}} \sin(\mathrm{PH_i})}{2} \end{bmatrix} \tag{2}$$

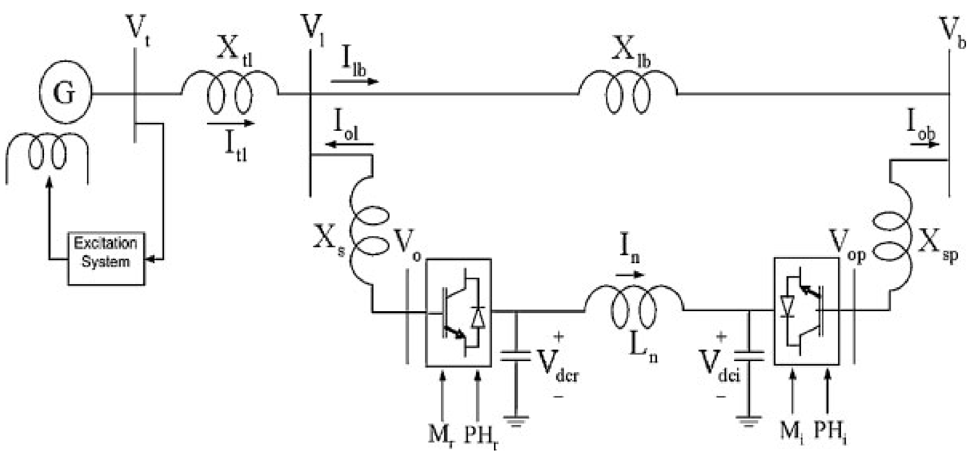

Figure 1. Configuration of case study.

DOI: 10.1002/etep

$$C_{\mathrm{dcr}}\frac{\mathrm{d}V_{\mathrm{dcr}}}{\mathrm{d}t} = -I_{\mathrm{n}} - \frac{M_{\mathrm{r}}}{2}\left[I_{\mathrm{old}}\cos(\mathrm{PH_r}) + I_{\mathrm{olq}}\sin(\mathrm{PH_r})\right] \tag{3}$$

$$L_{\mathrm{n}}\frac{\mathrm{d}I_{\mathrm{n}}}{\mathrm{d}t} = V_{\mathrm{dcr}} - V_{\mathrm{dci}} \tag{4}$$

$$C_{\mathrm{dci}}\frac{\mathrm{d}V_{\mathrm{dci}}}{\mathrm{d}t} = I_{\mathrm{n}} - \frac{M_{\mathrm{i}}}{2}\left(I_{\mathrm{obd}}\cos(\mathrm{PH_i}) + I_{\mathrm{obq}}\sin(\mathrm{PH_i})\right) \tag{5}$$

Where V_{l}, V_{b}, I_{ol}, and I_{ob} are the middle bus voltage, infinite bus voltage, flowed current from rectifier and inverter, respectively. C_{dcr}, C_{dci} and V_{dcr}, V_{dci} are the DC link capacitances and voltages, respectively. L_{n} is the DC link inductance.The nonlinear model of the SMIB system of Figure 1 is:

$$\dot{\delta} = \omega_{\mathrm{b}}\omega \tag{6}$$

$$\dot{\omega} = \frac{(P_{\mathrm{m}} - P_{\mathrm{e}} - D\omega)}{M} \tag{7}$$

$$\dot{E}'_{\mathrm{q}} = \frac{(E_{\mathrm{fd}} - E_{\mathrm{q}})}{T'_{\mathrm{do}}} \tag{8}$$

$$\dot{E}_{\mathrm{fd}} = \frac{(K_{\mathrm{A}}(V_{\mathrm{ref}} - V_{\mathrm{t}}) - E_{\mathrm{fd}})}{T_{\mathrm{A}}} \tag{9}$$

Where:$P_{\mathrm{e}} = V_{\mathrm{td}}I_{\mathrm{tld}} + V_{\mathrm{tq}}I_{\mathrm{tlq}}$, $V_{\mathrm{t}} = \sqrt{V_{\mathrm{td}}^2 + V_{\mathrm{tq}}^2}$, $V_{\mathrm{td}} = x_{\mathrm{q}}I_{\mathrm{tlq}}$, $V_{\mathrm{tq}} = E'_{\mathrm{q}} - x'_{\mathrm{d}}I_{\mathrm{tld}}$, $I_{\mathrm{lbd}} = I_{\mathrm{old}} + I_{\mathrm{tld}}$, $I_{\mathrm{lbq}} = I_{\mathrm{olq}} + I_{\mathrm{tlq}}$, $E_{\mathrm{q}} = (x_{\mathrm{d}} - x'_{\mathrm{d}})I_{\mathrm{tld}} + E'_{\mathrm{q}}$where P_{m} (is equal input torque, T_{m} in per unit system) and P_{e} are the input and output power, respectively, M and D the inertia constant and damping coefficient, respectively, ω_{b} the synchronous speed, δ and ω the rotor angle and speed, respectively, E'_{q}, E_{fd} and V_{t} the generator internal, field, and terminal voltages, respectively, $T'_{\mathrm{do}}$the open circuit field time constant, X_{d}, X'_{d}, and X_{q} the d-axis, d-axis transient reactance, and *q*-axis reactance, respectively, K_{A} and T_{A} the exciter gain and time constant, respectively, V_{ref} the reference voltage.

Also, from Figure 1 we have:

$$\bar{V}_{\mathrm{t}} = jX_{\mathrm{tl}}\bar{I}_{\mathrm{tl}} + \bar{V}_{\mathrm{l}} \tag{10}$$

$$\bar{V}_{\mathrm{t}} = jX_{\mathrm{tl}}\bar{I}_{\mathrm{tl}} + jX_{\mathrm{lb}}\bar{I}_{\mathrm{lb}} + \bar{V}_{\mathrm{b}} \tag{11}$$

$$\bar{I}_{\mathrm{lb}} = \bar{I}_{\mathrm{tl}} + \frac{\bar{V}_{\mathrm{o}} - \bar{V}_{\mathrm{t}} + jX_{\mathrm{tl}}\bar{I}_{\mathrm{tl}}}{jX_{\mathrm{s}}} \tag{12}$$

Where $\bar{I}_{\mathrm{tl}}$, $\bar{V}_{\mathrm{o}}$, $\bar{I}_{\mathrm{lb}}$, and $\bar{V}_{\mathrm{b}}$are the armature current, rectifier voltage, infinite bus current and voltage, respectively. From Equations (10) and (11) we could have:

$$I_{\mathrm{tlq}} = \frac{\frac{X_{\mathrm{lb}}}{X_{\mathrm{s}}}\frac{M_{\mathrm{r}}}{2}V_{\mathrm{dcr}}\cos(\mathrm{PH_r}) + V_{\mathrm{b}}\sin(\delta)}{ZX_{\mathrm{q}} + A} \tag{13}$$

$$I_{\mathrm{tld}} = \frac{ZE'_{\mathrm{q}} - \frac{X_{\mathrm{lb}}}{X_{\mathrm{s}}}\frac{M_{\mathrm{r}}}{2}V_{\mathrm{dcr}}\sin(PH_{\mathrm{r}}) - V_{\mathrm{b}}\cos(\delta)}{ZX'_{\mathrm{d}} + A} \tag{14}$$

DOI: 10.1002/etep

And for inverter side:

$$I_{obd} = \frac{\frac{M_i}{2} V_{dci} \sin(PH_i) - V_b \cos(\delta)}{X_{sp}} \tag{15}$$

$$I_{obq} = \frac{V_b \sin(\delta) - \frac{M_i}{2} V_{dci} \cos(PH_i)}{X_{sp}} \tag{16}$$

2.2. *Linearization of nonlinear state space equations*

The neural damping controller must be designed at a nonlinear dynamic model of power system. However, the nonlinear dynamic model is linearized in order to select the most effective input control signals and design of phase compensator.By linearizing Equations (1)–(9), (13)–(16):

$$\Delta\dot{\delta} = \omega_b \Delta\omega \tag{17}$$

$$\Delta\dot{\omega} = \frac{(\Delta P_m - \Delta P_e - D\Delta\omega)}{M} \tag{18}$$

$$\Delta\dot{E}'_q = \frac{(\Delta E_{fd} - \Delta E_q)}{T'_{do}} \tag{19}$$

$$\Delta\dot{E}_{fd} = \frac{(-K_A \Delta V_t - \Delta E_{fd})}{T_A} \tag{20}$$

Where:

$$\Delta V_t = K_5 \Delta\delta + K_6 \Delta E'_q + K_{Vdcr} \Delta V_{dcr} + K_{VM_r} \Delta M_r + K_{VPH_r} \Delta PH_r \tag{21}$$

$$\Delta P_e = K_1 \Delta\delta + K_2 \Delta E'_q + K_{pdcr} \Delta V_{dcr} + K_{pM_r} \Delta M_r + K_{pPH_r} \Delta PH_r \tag{22}$$

$$\Delta E_q = K_3 \Delta E'_q + K_4 \Delta\delta + K_{qPH_r} \Delta PH_r + K_{qM_r} \Delta M_r + K_{qdcr} \Delta V_{dcr} \tag{23}$$

$$C_{dcr}\, \Delta\dot{V}_{dcr} = -\Delta I_n + q_1 \Delta\delta + q_2 \Delta E'_q + q_3 \Delta V_{dcr} + q_4 \Delta M_r + q_5 \Delta PH_r \tag{24}$$

$$C_{dci}\, \Delta\dot{V}_{dci} = \Delta I_n + q_6 \Delta\delta + q_7 \Delta V_{dci} + q_8 \Delta M_i + q_9 \Delta PH_i \tag{25}$$

From Equations (1)–(5) and substituting (21)–(23) in (17)–(20), we can obtain the state variable of the power system installed with the VSC HVDC to be:

$$\Delta\dot{X} = A\Delta X + B\Delta U$$

and

$$\begin{aligned} \Delta X &= [\Delta\delta, \Delta\omega, \Delta E'_q, \Delta E_{fd}, \Delta V_{dcr}, \Delta V_{dci}, \Delta I_n]^T \\ \Delta U &= [\Delta M_r, \Delta PH_r, \Delta M_i, \Delta PH_i]^T \end{aligned} \tag{26}$$

DOI: 10.1002/etep

Where:

$$A = \begin{bmatrix} 0 & \omega_b & 0 & 0 & 0 & 0 & 0 \\ -\frac{K_1}{M} & -\frac{D}{M} & -\frac{K_2}{M} & 0 & -\frac{K_{\text{pdcr}}}{M} & 0 & 0 \\ -\frac{K_4}{T'_{\text{do}}} & 0 & -\frac{K_3}{T'_{\text{do}}} & \frac{1}{T'_{\text{do}}} & -\frac{K_{\text{qdcr}}}{T'_{\text{do}}} & 0 & 0 \\ -\frac{K_A K_5}{T_A} & 0 & -\frac{K_A K_6}{T_A} & -\frac{1}{T_A} & -\frac{K_A K_{V\text{dcr}}}{T_A} & 0 & 0 \\ \frac{q_1}{C_{\text{dcr}}} & 0 & \frac{q_2}{C_{\text{dcr}}} & 0 & \frac{q_3}{C_{\text{dcr}}} & 0 & -\frac{1}{C_{\text{dcr}}} \\ \frac{q_6}{C_{\text{dci}}} & 0 & 0 & 0 & 0 & \frac{q_7}{C_{\text{dci}}} & -\frac{1}{C_{\text{dci}}} \\ 0 & 0 & 0 & 0 & 0 & \frac{1}{L_n} & -\frac{1}{L_n} \end{bmatrix}$$

$$B = \begin{bmatrix} 0 & 0 & 0 & 0 \\ -\frac{K_{\text{p}M_r}}{M} & -\frac{K_{\text{pPH}_r}}{M} & 0 & 0 \\ -\frac{K_{\text{q}M_r}}{T'_{\text{do}}} & -\frac{K_{\text{qPH}_r}}{T'_{\text{do}}} & 0 & 0 \\ -\frac{K_{VM_r}}{T_A} & -\frac{K_{V\text{PH}_r}}{T_A} & 0 & 0 \\ \frac{q_4}{C_{\text{dcr}}} & \frac{q_5}{C_{\text{dcr}}} & 0 & 0 \\ 0 & 0 & \frac{q_8}{C_{\text{dci}}} & \frac{q_9}{C_{\text{dci}}} \\ 0 & 0 & 0 & 0 \end{bmatrix}$$

Where ΔM_i, ΔM_r, ΔPH_i, and ΔPH_r are the linearization of the input control signals of the VSC HVDC. The dynamic model of Equation (26), namely Phillips–Heffron model can be shown by Figure 2. In this figure K_{pu}, K_{qu}, K_{vu}, K_{q}, K_{p}, and ΔU are defined below:

$$\begin{aligned} K_{\text{pu}} &= \left[K_{\text{p}M_r}, K_{\text{pPH}_r}, 0, 0\right]' \\ K_{\text{qu}} &= \left[K_{\text{q}M_r}, K_{\text{qPH}_r}, 0, 0\right]' \\ K_{\text{vu}} &= \left[K_{VM_r}, K_{V\text{PH}_r}, 0, 0\right]' \\ K_{\text{q}} &= \left[\frac{q_4}{C_{\text{dcr}}}, \frac{q_5}{C_{\text{dcr}}}, 0, 0\right]' \\ K_{\text{p}} &= \left[0, 0, \frac{q_8}{C_{\text{dci}}}, \frac{q_9}{C_{\text{dci}}}\right] \end{aligned}$$

It can be seen that the configuration of the Phillips–Heffron model is exactly the same as that installed with SVC, TCSC, TCPS, UPFC and STATCOM.

Also from Equation (26), it can be seen that there are four choices of input control signals (ΔM_i, ΔM_r, ΔPH_i and ΔPH_r) of the VSC HVDC to add on the damping controller output. Therefore, in designing the damping controller, besides setting its parameters, the selection of the input control signal to superimpose on the damping controller output is also important.

3. CONTROLLABILITY MEASURE

To measure the controllability of the electromechanical (EM) mode by a given input (control signal), the SVD is employed [12]. Mathematically, if **G** is an $m \times n$ complex matrix, then there exist unitary matrices **U** and **V** with dimensions of $m \times m$ and $n \times n$, respectively, such that:

$$\mathbf{G} = \mathbf{U}\Sigma\mathbf{V}^{\text{H}} \tag{27}$$

Where

$$\Sigma = \begin{bmatrix} \Sigma_1 & 0 \\ 0 & 0 \end{bmatrix}, \ \Sigma_1 = \text{diag}(\sigma_1, ..., \sigma_r)$$

With $\sigma_1 \geq \ldots \geq \sigma_r \geq 0$ where $r = \min\{m, n\}$ and $\sigma_1, \ldots, \sigma_r$ are the singular values of **G**.

DOI: 10.1002/etep

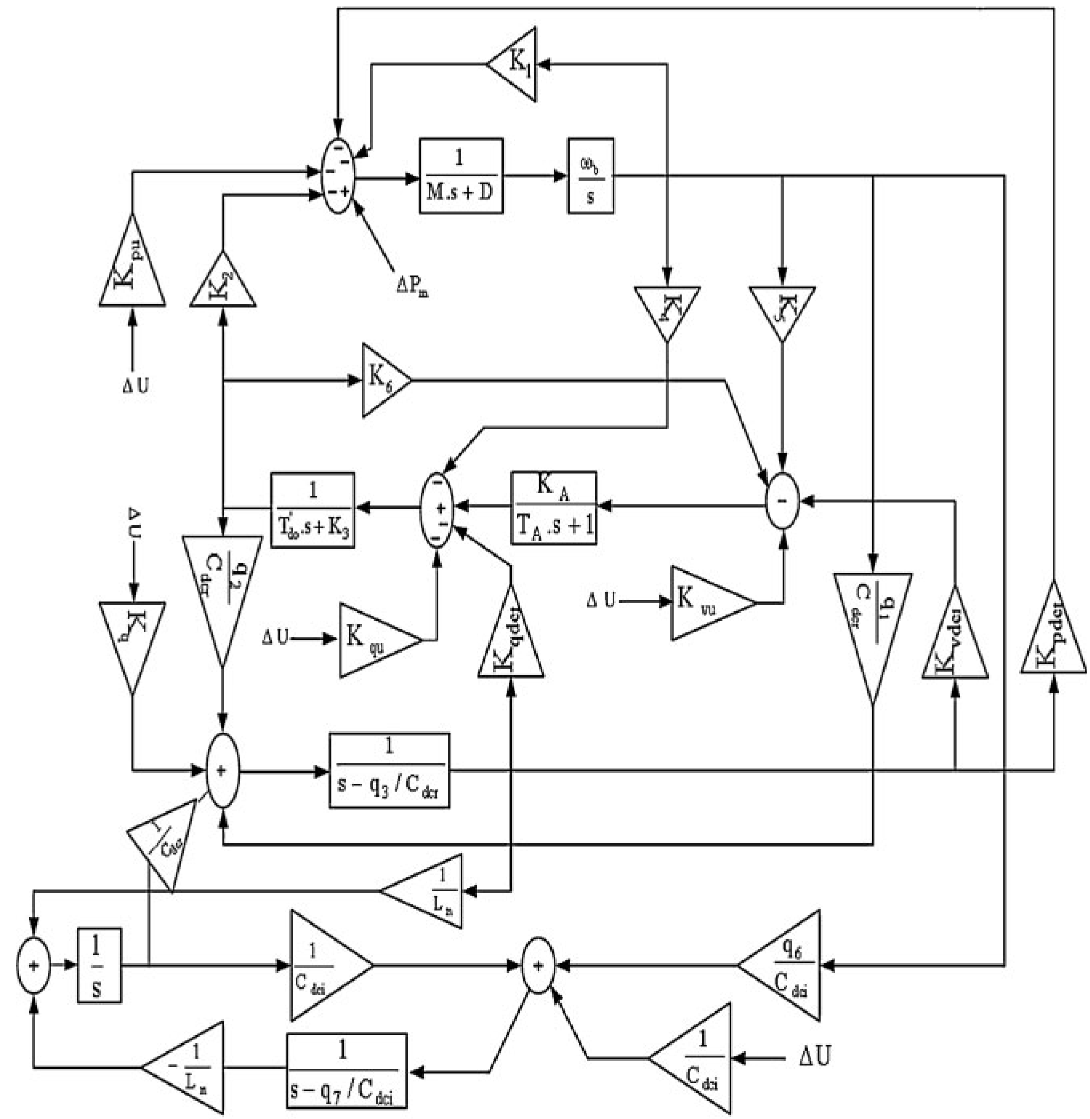

Figure 2. Phillips–Heffron model of power system installed with HVDC.

The minimum singular value σ_r represents the distance of the matrix **G** from all the matrices with a rank of $r-1$[13]. This property can be used to quantify modal controllability [10]. The matrix **B** can be written as $\mathbf{B} = [h_1\ h_2\ h_3\ h_4]$ where h_i is a column vector corresponding to the ith input. The minimum singular value, $\sigma_{\min}$ of the matrix $[\lambda I\text{–}A, h_i]$ indicates the capability of the ith input to control the mode associated with the eigenvalue λ. Actually, the higher $\sigma_{\min}$, the higher the controllability of this mode by the input control considered. As a result, the controllability of the EM mode can be examined with all inputs in order to identify the most effective one to control the mode.

4. DESIGN OF DAMPING CONTROLLERS

4.1. Conventional phase compensator

The damping controllers are designed to produce an electrical torque in phase with the speed deviation. The four control parameters of the HVDC (ΔM_{i}, ΔM_{r}, $\Delta \mathrm{PH}_{\mathrm{i}}$ and $\Delta \mathrm{PH}_{\mathrm{r}}$) can be modulated in order to produce the damping torque. The speed deviation (the output of Phillips–Heffron model in Figure 2) is considered as the input to the damping controllers.

DOI: 10.1002/etep

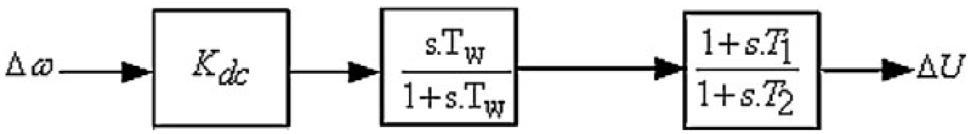

Figure 3. Structure of lead–lag controller.

The output of this controller is added to one of input control signals and the other signals have been considered zero, as a result the Phillips–Heffron model in Figure 2 is single input and single output (SISO).

The structure of HVDC based damping controller is shown in Figure 3. It consists of gain, signal washout, and phase compensator blocks. The parameters of the damping controller are obtained using the phase compensation technique. The detailed step-by-step procedure for computing the parameters of the damping controllers using phase compensation technique is given below [8,14]:

4.2. *Proposed adaptive neural damping controller*

The power system linearized model at a given operating point in Figure 2 cannot be appropriate during the severe disturbances like the faults. Also, conventional phase compensator based this model may have unacceptable response in nonlinear power system model. So in this paper an adaptive neural controller [8,11] is proposed to use in nonlinear model of VSC HVDC in Figure 1 (Equations (1)–(16)) and linear model in Figure 2 as shown in Figure 4. This adaptive neural controller consists of two separate neural networks as identifier and controller described in following sections.

4.2.1. Neural identifier. Structure of neural identifier is shown in Figure 5. This network has four neurons at hidden layer and one at output layer. Activation function is *f* that is hyperbolic tangent. It is

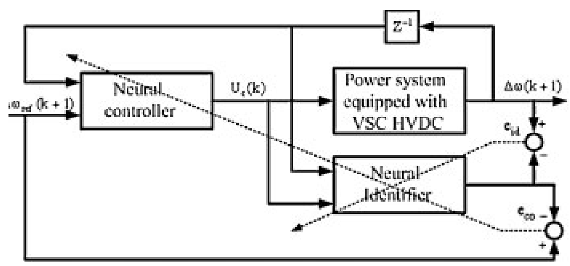

Figure 4. Proposed adaptive neural damping controller.

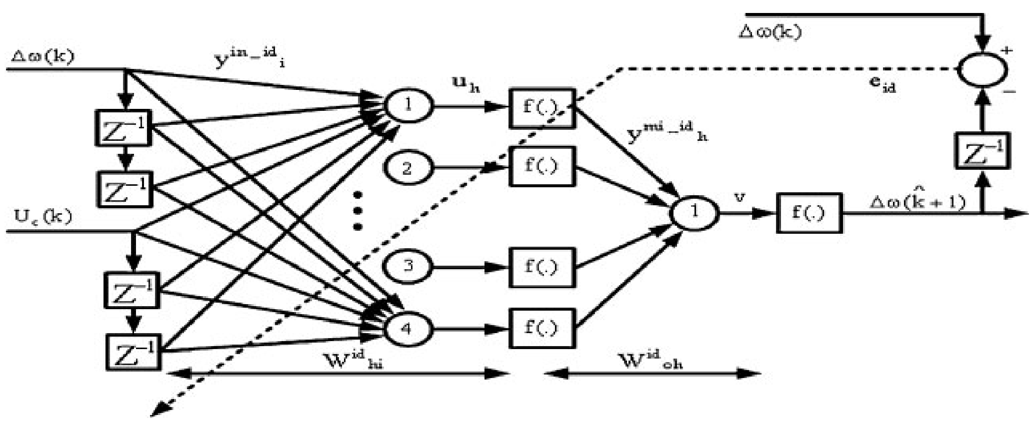

Figure 5. Structure of the online neural identifier.

DOI: 10.1002/etep

trained using error back propagation method. Cost function is defined as:

$$E_{\mathrm{id}} = \frac{1}{2}(\Delta\omega - \hat{\Delta\omega})^2 = \frac{1}{2}{e_{\mathrm{id}}}^2 \tag{28}$$

$\Delta\omega$ and $\hat{\Delta\omega}$ are power system (i.e., rotor speed deviation) and neural identifier output, respectively.

$$\frac{\partial E_{\mathrm{id}}}{\partial(\hat{\Delta\omega})} = -(\Delta\omega - \hat{\Delta\omega}) = -e_{\mathrm{id}} \tag{29}$$

And,

$$\frac{\partial E_{\mathrm{id}}}{\partial w_{\mathrm{oh}}^{\mathrm{id}}} = \frac{\partial E_{\mathrm{id}}}{\partial e_{\mathrm{id}}} \frac{\partial e_{\mathrm{id}}}{\partial(\hat{\Delta\omega})} \frac{\partial(\hat{\Delta\omega})}{\partial v} \frac{\partial v}{\partial w_{\mathrm{oh}}^{\mathrm{id}}} \tag{30}$$

Where $w_{\mathrm{oh}}^{\mathrm{id}}$ are weights between output and hidden layer. Using Equation (30), the sensitive coefficient of output neuron is calculated and output weights are updated according to Equation (31).

$$w_{\mathrm{oh_{New}}}^{\mathrm{id}} = w_{\mathrm{oh}\,\mathrm{Old}}^{\mathrm{id}} - \eta \frac{\partial E_{\mathrm{id}}}{\partial w_{\mathrm{oh}}^{\mathrm{id}}} \tag{31}$$

Using sensitive coefficient in output neuron, it is possible to correct other weights between hidden and input layer.

4.2.2. Neural controller. Structure of neural controller is shown in Figure 6. This is a feed forward network including four neurons at hidden and one neuron at output layer. Back propagation method used to train this network is described as follows.

Cost function to training this network is:

$$E_{\mathrm{co}} = \frac{1}{2}(0 - \hat{\Delta\omega})^2 = \frac{1}{2}\hat{\Delta\omega}^2 = \frac{1}{2}{e_{\mathrm{co}}}^2 \tag{32}$$

And

$$\frac{\partial E_{\mathrm{co}}}{\partial(\hat{\Delta\omega})} = \hat{\Delta\omega} = -e_{\mathrm{co}} \tag{33}$$

$$\frac{\partial E_{\mathrm{co}}}{\partial w_{\mathrm{oh}}^{\mathrm{co}}} = \frac{\partial E_{\mathrm{co}}}{\partial e_{\mathrm{co}}} \frac{\partial e_{\mathrm{co}}}{\partial(\hat{\Delta\omega})} \frac{\partial(\hat{\Delta\omega})}{\partial v} \frac{\partial v}{\partial w_{\mathrm{oh}}^{\mathrm{co}}} \tag{34}$$

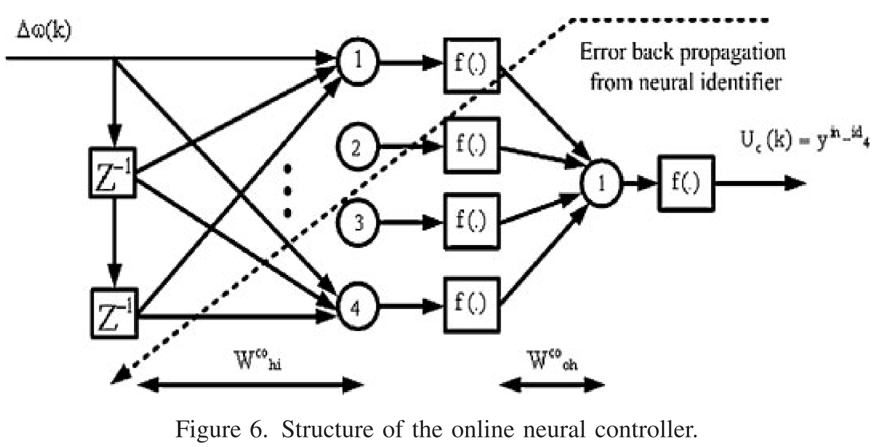

Figure 6. Structure of the online neural controller.

DOI: 10.1002/etep

V, $w_{\text{oh}}^{\text{co}}$ are the neural identifier output and the weights between output and hidden layer of neural controller, respectively.

$$\begin{aligned} v &= \sum_h w_{\text{oh}}^{\text{id}} y_h^{\text{mi\_id}} \\ y_h^{\text{mi\_id}} &= f\Big(\sum_i w_{\text{hi}}^{\text{id}} y_i^{\text{in\_id}}\Big) = f(u_h) \end{aligned} \tag{35}$$

$y_i^{\text{in\_id}}, y_h^{\text{mi\_id}}, w_{\text{hi}}^{\text{id}}, w_{\text{oh}}^{\text{id}}$, i and h are inputs, inputs to output layer, connection weights between input and hidden layer, weights between output and hidden layer, number of inputs and number of neuron in hidden layer of neural identifier, respectively.

where:

$$\frac{\partial v}{\partial w_{\text{oh}}^{\text{co}}} = \frac{\partial v}{\partial U_{\text{c}}} \frac{\partial U_{\text{c}}}{\partial w_{\text{oh}}^{\text{co}}} = \frac{\partial v}{\partial y_h^{\text{mi\_id}}} \frac{\partial y_h^{\text{mi\_id}}}{\partial U_{\text{c}}} \frac{\partial U_{\text{c}}}{\partial w_{\text{oh}}^{\text{co}}} \tag{36}$$

Using Equations (34)–(36), it is possible to calculate the sensitive coefficient in output neuron of neural controller and correct the middle and output weights of neural controller.

5. SIMULATION RESULTS

Damping controller information and test system parameters are given in Appendix A and B, respectively. Constant coefficients in Equation (26) are calculated according to information which are given in Appendix C for a given operating point.

The Phillips–Heffron model based on VSC HVDC in Figure 2 and nonlinear model of Equations (1)–(16) have been modeled by MATLAB/SIMULINK to demonstrate the damping controllers on power system oscillation stability.

5.1. Controllability measure

SVD is employed to measure the controllability of the EM mode from each of the four inputs, ΔM_{r}, $\Delta \text{PH}_{\text{r}}$, ΔM_{i}, $\Delta \text{PH}_{\text{i}}$ in Figure 2 for several operating points. The minimum singular value $\sigma_{\min}$ is estimated over a wide range of operating conditions. For SVD analysis, P_{e} ranges from 0.01 to 1.5 pu and $Q_{\text{e}} = 0.4$ pu. At these loading conditions, the parameters of Phillips–Heffron model in Figure 2 are calculated according to Appendix C, the EM mode is identified, and the SVD-based controllability measure is implemented. For comparison purposes, the minimum singular value for all inputs at $Q_{\text{e}} = 0.4$ pu is shown in Figure 7, respectively. From these figures, the following can be noticed:

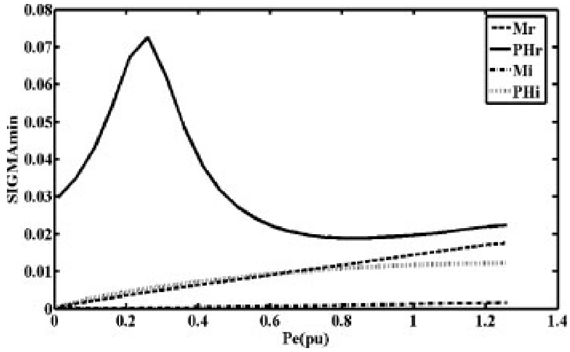

Figure 7. Controllability measure using SVD.

DOI: 10.1002/etep

Table I. Synchronous machine condition.

Operating condition	P_e	Q_e	V_t
λ_1 (Nominal)	1	0.015	1
λ_2 (Heavy)	1.1	0.3	1

- EM mode controllability *via* PH_r is always higher than that of any other input.
- The capabilities of PH_r and M_r to control the EM mode is higher than that of PH_i and M_i.
- The EM mode is controllable with PH_i than with M_i.

5.2. *Testing proposed supplementary controllers*

To assess the effectiveness of the proposed stabilizers two different operating conditions are considered according to Table I.

The parameters of designed phase compensator are $T_1 = 0.1522$, $T_2 = 0.3592$, $K_{dc} = -23.5$. This controller is designed for nominal operating condition and it is applied to ΔPH_r according to SVD result in Fig. 7. The supplementary neural networks weights are selected randomly from 0 to 1.

Testing linear model (Fig. 2) consists of small changing in mechanical power ($\Delta P_m = 0.05$) at $t = 0$ s. Testing nonlinear model (equations (1)–(16)) includes three phase fault at infinite bus at $t = 1$ s that is removed after 7 cycles and step changing in mechanical power ($\Delta P_m = 0.1$) at $t = 1$ s.

Figures 8–9 show the linear power system responses in conditions λ_1 and λ_2, respectively. According to these figures, neural damping controller damps active power and rotor speed oscillations better than conventional phase compensator for small disturbances, so neural damping controller improves dynamical stability. Figures 10–11 show the nonlinear power responses for suddenly step changing in mechanical power ($\Delta P_m = 0.1$) at $t = 1$ s. It is clearly seen that the dynamical performance at different loading conditions for a neural damping controller has more quality because neural controller decreases settling time and peak amplitude. Figure 11 shows the phase compensator cannot stabilize system as its parameters are set around λ_1. In Figures 12–14a three-phase fault at $t = 1$ second occurs and clears after 7 cycles. It is considered that phase compensator cannot damp oscillations for large disturbances, however neural damping controller has a good response in all operating conditions. As a result, neural controller improves dynamical and transient stability effectively.

5.2.1. *Linear power system response in λ_1 and $\Delta P_m = 0.05$.*

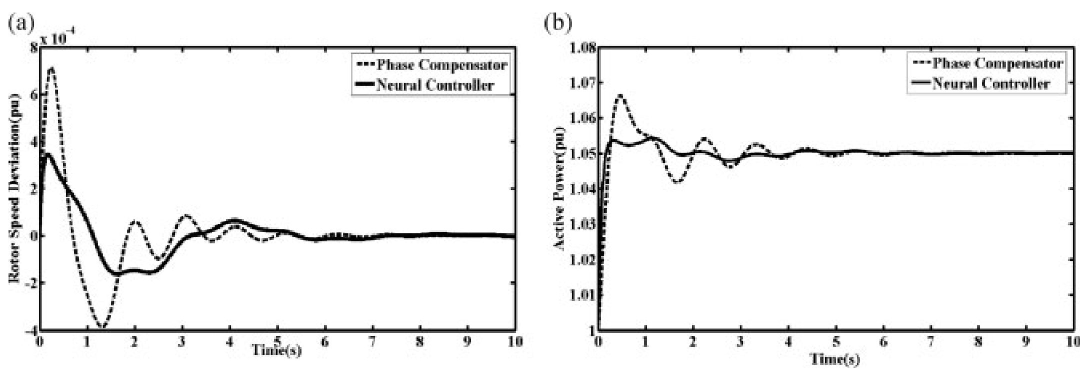

Figure 8. (a) Rotor speed deviation; (b) Active power.

DOI: 10.1002/etep

5.2.2. Linear power system response in λ_2 and $\Delta P_m = 0.05$.

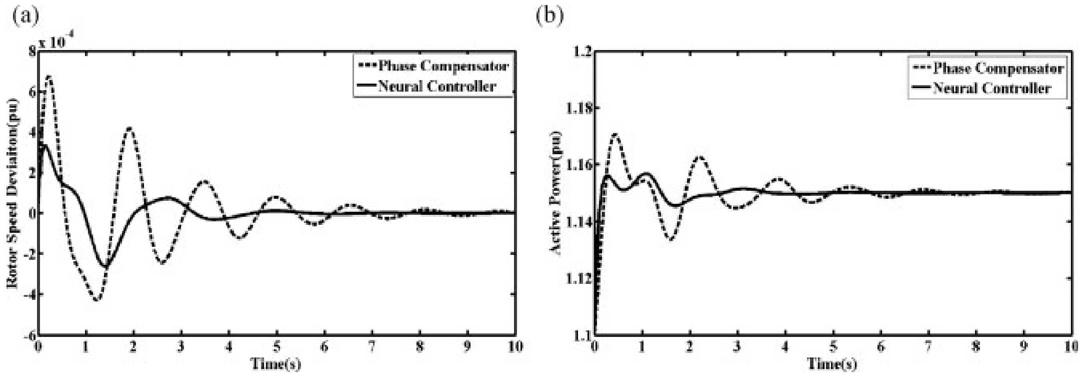

Figure 9. (a) Rotor speed deviation; (b) Active power.

5.2.3. Nonlinear power system response in λ_1 and $\Delta P_m = 0.1$.

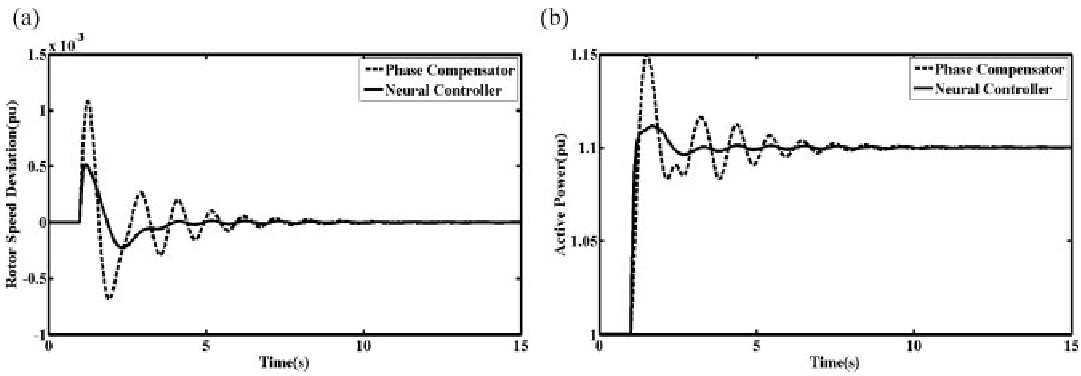

Figure 10. (a) Rotor speed deviation; (b) Active power.

5.2.4. Nonlinear power system response in λ_2 and $\Delta P_m = 0.1$.

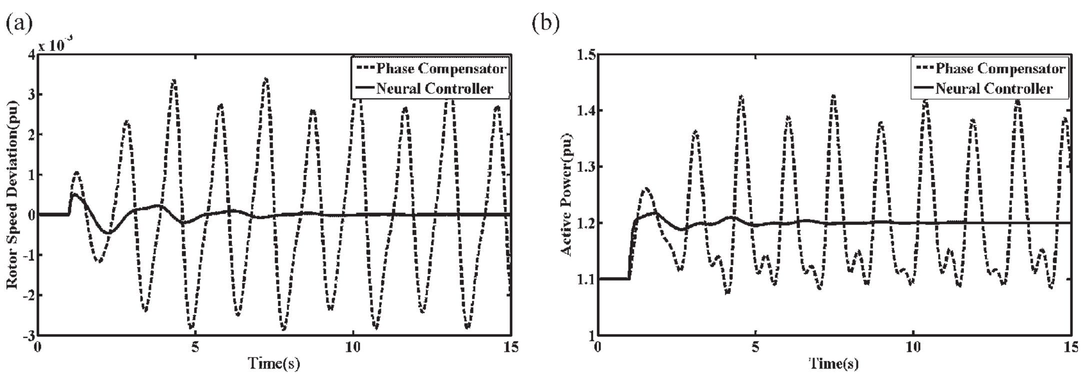

Figure 11. (a)Rotor speed deviation; (b) Active power.

DOI: 10.1002/etep

5.2.5. Nonlinear power system response in λ_1 and three-phase fault in infinite bus.

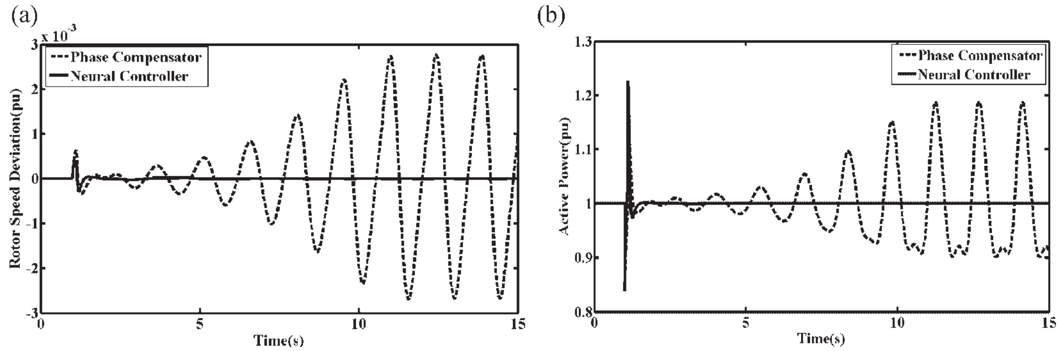

Figure 12. (a) Rotor speed deviation; (b) Active power.

5.2.6. Nonlinear power system response in λ_2 and three-phase fault in infinite bus.

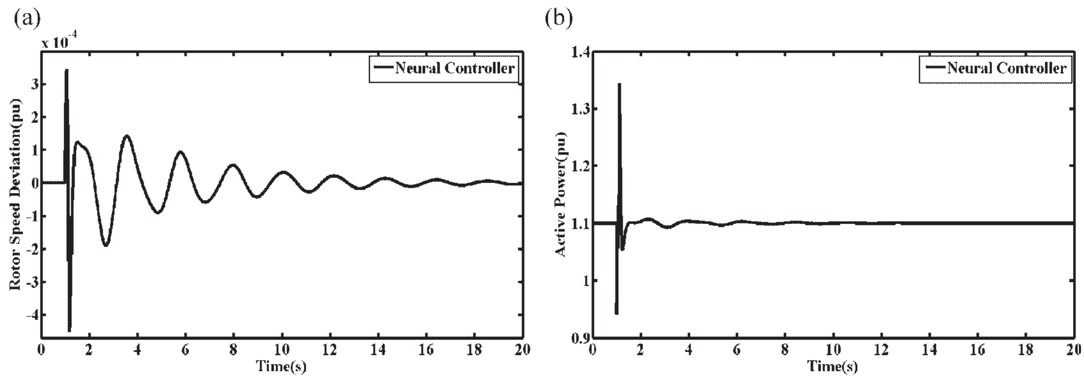

Figure 13. (a) Rotor speed deviation. (b) Active power.

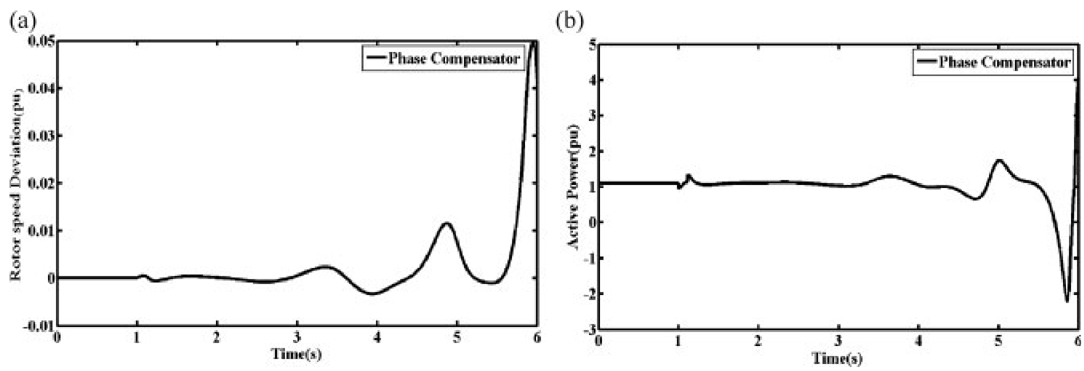

Figure 14. (a) Rotor speed deviation. (b) Active power.

6. CONCLUSION

In this paper, a novel dynamical model has been considered and supplementary controller has been designed to improve power system stability and oscillation damping. SVD has been employed to evaluate the EM mode controllability to the four VSC HVDC inputs. SVD illustrated that the EM mode has best controllability *via* the phase angle of rectifier. Also, for improving the system stability and damping oscillations, a neural damping controller has been proposed. The simulation results carried

DOI: 10.1002/etep

out by SIMULINK/MATLAB show neural damping controller has the perfect effect in dynamical and transient improvement in comparison with phase compensator.

REFERENCES

1. Villablanca M, Valle JD, Rojas J, Abarca J, Rojas W. A modified back-to-back HVDC system for 36-pulse operation. *IEEE Transactions on Power Delivery* 2000; **15**(2): 641–645.
2. Hammad A, Taylor C. HVDC controllers for system dynamic performance. *IEEE Transactions on Power Systems* 1991; **6**(2): 743–752.
3. Huang GM, Krishnaswamy V. HVDC controls for power system stability. *IEEE Power Engineering Society Summer Meeting* 2002; **1**: 597–602.
4. Baker M, Abbott K, Gemmell B. Frequency and system damping assistance from HVDC and FACTS controller. *Power Engineering Society Summer Meeting, 2002 IEEE,* 2002; **2**: 770–773.
5. Saeedifard M, Nikkhajoei H, Iravani R, Bakhshai A. A space vector modulation approach for a multimodule HVDC converter system. *IEEE Transactions on Power Delivery* 2007; **22**(3): 1643–1654.
6. Wang HF, Swift FJ. A unified model for the analysis of FACTS devices in damping power system oscillations part I: single-machine infinite-bus power systems. *IEEE Transactions on Power Delivery* 1997; **12**(2): 941–946.
7. Uzunovic E, Cãnizares CA, Reeve J. EMTP studies of UPFC power oscillation damping. *Proceedings of NAPS'99*, California, 1999; 155–163.
8. Liu. W, Venayagamoorthy G, Wunsch D. Adaptive neural network based power system stabilizer design. *IEEE, Neural networks, Proceeding of the international joint conference*, 2003; 4: 2970–2975.
9. Chia-Chi Chu, Hung-Chi Tsai. Application of Lyapunov-based adaptive neural network UPFC damping controllers for transient stability enhancement. *Power and Energy Society General Meeting—Conversion and Delivery of Electrical Energy*, IEEE, 20–24 July 2008; 1–6.
10. Shamsollahi P, Malik OP. Application of neural adaptive power system stabilizer in a multi-machine power system. *IEEE Transactions on Energy Conversion* 1999; **14**(3): 731–736.
11. Shamsollahi P, Malik OP. Real-time implementation and experimental studies of a neural adaptive power system stabilizer. *IEEE Transactions on Energy Conversion* 1999; **14**: 737–742.
12. Hamdan AMA. An investigation of the significance of singular value decomposition in power system dynamics. *Electrical Power and Energy Systems* 1999; **21**(6): 417–424.
13. Abdel-Magid YL, Abido MA. Robust coordinated design of excitation and TCSC-based stabilizers using genetic algorithm. *Electrical Power Systems Research* 2004; **69**: 129–141.
14. Larsen EV, Sanchez-Gasca JJ, Chow JH. Concepts for design of FACTS controllers to damp power swings. *IEEE Transactions on PWRS* 1995; **10**: 948–956.

APPENDIX A

Phase compensator: $T_1 = 0.1522$, $T_2 = 0.3592$, $K_{dc} = -23.5$.

Neural controller: two multilayer feed forward neural network with activation function: $a\tanh(bx)$. Hidden and output layer for identifier includes 4 and 1 neurons, respectively with $a = b = 1$, $\eta = 0.1$. Hidden and output layer for controller includes 3 and 1 neurons, respectively with $a = 20$, $b = 0.9$, $\eta = 0.1$.

APPENDIX B

The test system parameters are:

Machine and exciter:

$$X_d = 1,\quad X_q = 0.6,\quad X_d' = 0.3,\quad D = 0,\quad M = 8,$$
$$T_{do}' = 5.044,\quad \mathrm{freq} = 60,\quad v_{ref} = 1,\quad K_A = 140,\quad T_A = 0.015$$

Transmission line and transformer reactance:

$$X_{tl} = 0.18,\quad X_{lb} = 1,\quad X_{sp} = X_s = 0.18$$

VSC HVDC characteristics (pu):

$$V_{dcr} = V_{dci} = 3,\quad C_{dcr} = C_{dci} = 1,\quad L_n = 0.06$$

DOI: 10.1002/etep

APPENDIX C

Coefficients are:

$$Z = 1 + \frac{X_{\mathrm{lb}}}{X_{\mathrm{s}}}, \quad A = X_{\mathrm{tl}} + X_{\mathrm{lb}} + \frac{X_{\mathrm{tl}}}{X_{\mathrm{s}}}$$
$$[A] = A + ZX'_{\mathrm{d}}, \quad [B] = A + ZX_{\mathrm{q}}$$
$$C_1 = \frac{V_{\mathrm{b}}\cos(\delta)}{[B]}, \quad C_2 = -\frac{X_{\mathrm{lb}}M_{\mathrm{r}}V_{\mathrm{dc}}\sin(\mathrm{PH_r})}{2X_{\mathrm{s}}[B]}$$
$$C_3 = \frac{X_{\mathrm{lb}}V_{\mathrm{dc}}\cos(\mathrm{PH_r})}{2X_{\mathrm{s}}[B]}, \quad C_4 = \frac{X_{\mathrm{lb}}M_{\mathrm{r}}\cos(\mathrm{PH_r})}{2X_{\mathrm{s}}[B]}$$
$$C_5 = \frac{Z}{[A]}, \quad C_6 = \frac{V_{\mathrm{b}}\sin(\delta)}{[A]}$$
$$C_7 = -\frac{X_{\mathrm{lb}}M_{\mathrm{r}}V_{\mathrm{dc}}\cos(\mathrm{PH_r})}{2X_{\mathrm{s}}[A]}, \quad C8 = -\frac{X_{\mathrm{lb}}V_{\mathrm{dc}}\sin(\mathrm{PH_r})}{2X_{\mathrm{s}}[A]}$$
$$C_9 = -\frac{X_{\mathrm{lb}}M_{\mathrm{r}}V_{\mathrm{dc}}\cos(\mathrm{PH_r})}{2X_{\mathrm{s}}[A]}, \quad C_b = E'_{\mathrm{q}} + (X_{\mathrm{q}} - X'_{\mathrm{d}})$$
$$C_a = (X_{\mathrm{q}} - X'_{\mathrm{d}})I_{\mathrm{tlq}}, \quad K_1 = C_bC_1 + C_aC_6$$
$$K_2 = I_{\mathrm{tlq}}(1 + (X_{\mathrm{q}} - X'_{\mathrm{d}})C_5), \quad K_{\mathrm{pdcr}} = C_bC_4 + C_aC_9$$
$$K_{\mathrm{p}M_{\mathrm{r}}} = C_bC_3 + C_aC_8, \quad K_{\mathrm{pPH_r}} = C_bC_2 + C_aC_7$$
$$X_{\mathrm{d}} - X'_{\mathrm{d}} = J, \quad K_3 = 1 + JC_5, \quad K_4 = JC_6, K_{\mathrm{qPH_r}} = JC_7$$
$$K_{\mathrm{q}M_{\mathrm{r}}} = JC_8, \quad K_{\mathrm{qdcr}} = JC_9, \quad L = \frac{1}{V_{\mathrm{t}}}, \quad K_5 = L\Big(V_{\mathrm{td}}X_{\mathrm{q}}C_1 - V_{\mathrm{tq}}X'_{\mathrm{d}}C_6\Big)$$
$$K_6 = LV_{\mathrm{tq}}(1 - X'_{\mathrm{d}}C_5), \quad K_{V\mathrm{dcr}} = L(V_{\mathrm{td}}X_{\mathrm{q}}C_4 - V_{\mathrm{tq}}X'_{\mathrm{d}}C_9)$$
$$K_{VM_{\mathrm{r}}} = L(V_{\mathrm{td}}X_{\mathrm{q}}C_3 - V_{\mathrm{tq}}X'_{\mathrm{d}}C_8)$$
$$K_{V\mathrm{PH_r}} = L(V_{\mathrm{td}}X_{\mathrm{q}}C_2 - V_{\mathrm{tq}}X'_{\mathrm{d}}C_7), \quad E = \frac{X'_{\mathrm{d}} + X_{\mathrm{tl}}}{X_{\mathrm{s}}}, \quad F = \frac{X_{\mathrm{q}} + X_{\mathrm{tl}}}{X_{\mathrm{s}}}$$
$$C_{10} = EC_5 - \frac{1}{X_{\mathrm{s}}}, C_{11} = EC_6, C_{12} = EC_7 - \frac{M_{\mathrm{r}}}{2X_{\mathrm{s}}}V_{\mathrm{dcr}}\sin(\mathrm{PH_r})$$
$$C_{13} = \frac{1}{2X_s}M_{\mathrm{r}}\cos(\mathrm{PH_r}) + EC_8, \quad C_{14} = \frac{1}{2X_{\mathrm{s}}}\cos(\mathrm{PH_r}) + EC_9$$
$$C_{15} = FC_1, \quad C_{16} = \frac{1}{2X_{\mathrm{s}}}V_{\mathrm{dcr}}\sin(\mathrm{PH_r}) + FC_2$$
$$C_{17} = -\frac{1}{2X_{\mathrm{s}}}M_{\mathrm{r}}\cos(\mathrm{PH_r}) + FC_4$$
$$C_{18} = FC_3 - \frac{1}{2X_{\mathrm{s}}}V_{\mathrm{dcr}}\cos(\mathrm{PH_r}), \quad C_{19} = \frac{1}{X_{\mathrm{sp}}}V_{\mathrm{bd}}$$
$$C_{20} = \frac{1}{2X_{\mathrm{sp}}}M_{\mathrm{i}}\sin(\mathrm{PH_i}), \quad C_{21} = \frac{1}{2X_{\mathrm{sp}}}V_{\mathrm{dcr}}\sin(\mathrm{PH_i})$$
$$C_{22} = \frac{1}{2X_{\mathrm{sp}}}M_{\mathrm{i}}V_{\mathrm{dci}}\cos(\mathrm{PH_i}), \quad C_{23} = \frac{1}{X_{\mathrm{sp}}}V_{\mathrm{bq}}$$
$$C_{24} = -\frac{1}{2X_{\mathrm{sp}}}M_{\mathrm{i}}\cos(\mathrm{PH_i}), \quad C_{25} = -\frac{1}{2X_{\mathrm{sp}}}V_{\mathrm{dci}}\cos(\mathrm{PH_i})$$
$$C_{26} = \frac{1}{2X_{\mathrm{sp}}}V_{\mathrm{dci}}\sin(\mathrm{PH_i})$$
$$f_1 = -\big[0.5\cos(\mathrm{PH_i})I_{\mathrm{obd}} + 0.5\sin(\mathrm{PH_i})I_{\mathrm{obq}}\big]$$
$$f_2 = -\big[-0.5\sin(\mathrm{PH_i})I_{\mathrm{obd}} + 0.5\cos(\mathrm{PH_i})I_{\mathrm{obq}}\big]$$
$$f_3 = -0.5M_{\mathrm{i}}\cos(\mathrm{PH_i}), \quad f_4 = -0.5M_{\mathrm{i}}\sin(\mathrm{PH_i})$$
$$f_5 = -\big[0.5\cos(\mathrm{PH_r})I_{\mathrm{old}} + 0.5\sin(\mathrm{PH_r})I_{\mathrm{olq}}\big]$$
$$f_6 = -\big[-0.5\sin(\mathrm{PH_r})I_{\mathrm{old}} + 0.5\cos(\mathrm{PH_r})I_{\mathrm{olq}}\big]$$
$$f_7 = -0.5M_{\mathrm{r}}\cos(\mathrm{PH_r}), \quad f_4 = -0.5M_{\mathrm{r}}\sin(\mathrm{PH_r})$$
$$q_1 = f_7C_{11} + f_8C_{15}, \quad q_2 = f_7C_{10}, \quad q_3 = f_7C_{14} + f_8C_{17}$$
$$q_4 = f_5 + f_7C_{13} + f_8C_{18}, \quad q_5 = f_6 + f_7C_{12} + f_8C_{16}$$
$$q_6 = f_3C_{19} + f_4C_{23}, \quad q_7 = f_3C_{20} + f_4C_{24}, \quad q_8 = f_1 + f_3C_{21} + f_4C_{25}$$
$$q_9 = f_2 + f_3C_{22} + f_4C_{26}$$

DOI: 10.1002/etep